

FAST AND ACCURATE COMPUTATION OF TIME-DOMAIN ACOUSTIC SCATTERING PROBLEMS WITH EXACT NONREFLECTING BOUNDARY CONDITIONS

LI-LIAN WANG¹, BO WANG² AND XIAODAN ZHAO¹

ABSTRACT. This paper is concerned with fast and accurate computation of exterior wave equations truncated via exact circular or spherical nonreflecting boundary conditions (NRBCs, which are known to be nonlocal in both time and space). We first derive analytic expressions for the underlying convolution kernels, which allow for a rapid and accurate evaluation of the convolution with $O(N_t)$ operations over N_t successive time steps. To handle the nonlocality in space, we introduce the notion of boundary perturbation, which enables us to handle general bounded scatters by solving a sequence of wave equations in a regular domain. We propose an efficient spectral-Galerkin solver with Newmark's time integration for the truncated wave equation in the regular domain. We also provide ample numerical results to show high-order accuracy of NRBCs and efficiency of the proposed scheme.

1. INTRODUCTION

Wave propagation and scattering problems in unbounded media arise from diverse application areas such as acoustics, aerodynamics, electromagnetics, antenna design, oceanography and among others (see, e.g., [15, 33, 10]). Various approaches have been proposed for their numerical studies that include the boundary element methods (cf. [7]), infinite element methods (cf. [14]), perfectly matched layers (PML) (cf. [5]), nonreflecting boundary condition methods (cf. [22, 18]), and among others (cf. [25, 37]). An essential ingredient for the latter approach is to truncate an unbounded domain to a bounded domain by imposing an exact or approximate nonreflecting (absorbing or transparent) boundary condition at the outer artificial boundary, where the NRBC is designed to prevent spurious wave reflection from the artificial boundary (cf. the review papers [15, 16] and the references therein). The frequency-domain approaches for e.g., the time-harmonic Helmholtz problems have been intensively investigated, while the time-domain simulations, which are capable of capturing wide-band signals and modeling more general material inhomogeneities and nonlinearities (cf. [3, 9]), have been relatively less studied.

Although some types of NRBCs based on different principles have been proposed (see, e.g., [12, 4, 39, 34, 35, 17, 18, 16]), a longstanding issue of time-domain computation is the efficient treatment for NRBCs that can scale and integrate well with the solver for the underlying truncated problem (cf. [38, 19]). In practice, if an accurate NRBC is imposed, the artificial boundary could be placed as close as possible to the scatter that can significantly reduce the computational cost. In this paper, we restrict our attention to the exact NRBC on the circular or spherical artificial boundary. One major difficulty lies in that such a NRBC is *global* in space and

1991 *Mathematics Subject Classification.* 35J05, 35L05, 65R10, 65N35, 65E05, 65M70.

Key words and phrases. Time-domain Dirichlet-to-Neumann map, nonreflecting boundary conditions, inverse Laplace transform, modified Bessel functions, convolution, spectral methods, Newmark's time integration.

¹ Division of Mathematical Sciences, School of Physical and Mathematical Sciences, Nanyang Technological University, 637371, Singapore. The research of the authors is partially supported by Singapore AcRF Tier 1 Grant RG58/08.

² College of Mathematics and Computer Science, Hunan Normal University, Changsha, Hunan 410081, China. This author would like to thank the Division of Mathematical Sciences of Nanyang Technological University for the hospitality during the visit.

time in nature, as it involves the Fourier/spherical harmonic expressions in space, and history dependence in time induced by a convolution. The convolution kernel, termed as *nonreflecting boundary kernel* (NRBK) in [2], is the inverse Laplace transform of an expression that includes the logarithmic derivative of a modified Bessel function. The rapid computation of the NRBK and convolution is of independent interest. Alpert, Greengard and Hagstrom [2] proposed a rational approximation of the logarithmic derivative with a least square implementation, which allows for a reduction of the summation of the poles from $O(\nu)$ to $O(\log \nu \log \frac{1}{\varepsilon})$ (where $\nu \gg 1$ is the order of the modified Bessel function and ε is a given tolerance), and a recursive convolution. Jiang and Greengard [20, 21] further considered some interesting applications to Schrödinger equations in one and two dimensions. Li [23] introduced a more accurate low order approximation of the three-dimensional NRBK at a slightly expensive cost, where the observation that the Laplace transform of the three-dimensional NRBK is exactly a rational function lies at the heart of this algorithm. However, in many cases, the expressions are *not* rational functions. For instance, the two-dimensional NRBK also contains the contributions from the branch-cut along the negative real axis (see Theorem 2.1 below). Lubich and Schädle [24] developed some fast algorithm for the temporal convolution with $O(N_t \log N_t)$ operations (over N_t successive time steps) arising from NRBCs with non-rational expressions for other equations (e.g., Schrödinger equations and damped wave equations).

In this paper, we derive an analytic formula for the NRBK based on a direct inversion of the Laplace transform by the residue theorem (see Theorem 2.1 below). In fact, Sofronov [35] presented some formulas of similar type by working on much more complicated expressions of the kernel in terms of Tricomi's confluent hypergeometric functions. We show that with these formulas, we can evaluate the temporal convolution recursively and rapidly with $O(N_t)$ operations and almost without extra memory for the history dependence. Moreover, the analytic expression provides a useful apparatus for the stability and convergence analysis. It is worthwhile to remark that Chen [6] reformulated the two-dimensional wave problem into a first-order system in time and showed the well-posedness of the truncated problem with an alternative formulation of the NRBC.

It is known that the nonlocality of the NRBC in space can be efficiently handled by Fourier/spherical harmonic expansions when the scatter is a disk or a ball. Recently, a systematic approach, based on the boundary perturbation technique (also called the *transformed field expansion* (TFE) method (cf. [28])), has been developed in [29, 13, 30] for time-harmonic Helmholtz equations in exterior domains with general bounded obstacles, under which the whole algorithm boils down to solving a sequence of Helmholtz equations in a 2-D annulus or a 3-D spherical shell. In this paper, we highlight that this notion can be extended to time-domain computation, though it has not been investigated before as far as we know. In this paper, we propose an efficient spectral-Galerkin method with Newmark's time integration for the truncated wave equations in an annulus or a spherical shell, and provide ample numerical results to show the efficiency of the solver and high accuracy of NRBC from several angles.

The rest of the paper is organized as follows. In Section 2, we present the formulation of NRBCs, and derive the analytic formulas for NRBKs. In Section 3, we present some properties of NRBK and analyze well-posedness of the truncated wave equation. In Section 4, we outline the notion of the TFE method and propose an efficient spectral-Galerkin and Newmark's time integration scheme for the truncated wave problem in regular domains. We provide ample numerical results in Section 5.

2. EVALUATION OF NONREFLECTING BOUNDARY KERNELS

In this paper, we consider the time-domain acoustic scattering problem with sound-soft boundary conditions on the bounded obstacle:

$$\partial_t^2 U = c^2 \Delta U + F, \quad \text{in } \Omega_\infty := \mathbb{R}^d \setminus \bar{D}, \quad t > 0, \quad d = 2, 3; \quad (2.1)$$

$$U = U_0, \quad \partial_t U = U_1, \quad \text{in } \Omega_\infty, \quad t = 0; \quad (2.2)$$

$$U = G, \quad \text{on } \Gamma_D, \quad t > 0; \quad \partial_t U + c \partial_{\mathbf{n}} U = o(|\mathbf{x}|^{(1-d)/2}), \quad |\mathbf{x}| \rightarrow \infty, \quad t > 0. \quad (2.3)$$

Here, D is a bounded obstacle (scatter) with Lipschitz boundary Γ_D , $c > 0$ is a given constant, and the radiation condition (2.3), where $\mathbf{n} = \mathbf{x}/|\mathbf{x}|$, corresponds to the well-known Sommerfeld radiation condition in the frequency domain. Assume that the data F, U_0 and U_1 are compactly supported in a 2-D disk or a 3-D ball B of radius b .

A common way is to reduce this exterior problem to the problem in a bounded domain by imposing an exact or approximate NRBC at the artificial boundary $\Gamma_b := \partial B$. In what follows, we shall focus on the wave equation truncated by the exact circular or spherical NRBC:

$$\partial_t^2 U = c^2 \Delta U + F, \quad \text{in } \Omega := B \setminus \bar{D}, \quad t > 0, \quad d = 2, 3; \quad (2.4)$$

$$U = U_0, \quad \partial_t U = U_1, \quad \text{in } \Omega, \quad t = 0; \quad U = G, \quad \text{on } \Gamma_D, \quad t > 0; \quad (2.5)$$

$$\partial_r U = T_d(U), \quad \text{at } r = b, \quad t > 0, \quad (2.6)$$

where $T_d(U)$ is the so-called time-domain DtN map.

2.1. Formulation of $T_d(U)$. We first present the expression of $T_d(U)$ in (2.6), and refer to e.g., [18, 3] (and the original references therein) for the detailed derivation. It is known that the problem (2.1)-(2.3), exterior to $D = B$ with $F = U_0 = U_1 \equiv 0$ and $G = U|_{r=b}$ (i.e., the Dirichlet data taken from the interior problem (2.4)-(2.6)), can be solved analytically by using Laplace transform in time and separation of variables in space in polar coordinate (r, ϕ) /spherical coordinate (r, θ, ϕ) . By imposing the continuity of directional derivative with respect to r across the artificial boundary $r = b$, we obtain the boundary condition (2.6) with

$$T_d(U) = \begin{cases} \left(-\frac{1}{c} \frac{\partial U}{\partial t} - \frac{U}{2r} \right) \Big|_{r=b} + \sum_{|n|=0}^{\infty} \sigma_n(t) * \hat{U}_n(b, t) e^{in\phi}, & d = 2, \\ \left(-\frac{1}{c} \frac{\partial U}{\partial t} - \frac{U}{r} \right) \Big|_{r=b} + \sum_{n=0}^{\infty} \sum_{|m|=0}^n \sigma_{n+1/2}(t) * \hat{U}_{nm}(b, t) Y_n^m(\theta, \phi), & d = 3, \end{cases} \quad (2.7)$$

where

$$\sigma_\nu(t) := \mathcal{L}^{-1} \left[\frac{s}{c} + \frac{1}{2b} + \frac{s}{c} \frac{K'_\nu(sb/c)}{K_\nu(sb/c)} \right], \quad \nu = n, n + 1/2. \quad (2.8)$$

Here, K_ν is the modified Bessel function of the second kind of order ν (see, e.g., [1, 40]), and $\mathcal{L}^{-1}[H(s)]$ is the inverse Laplace transform of a Laplace transformable function $h(t)$ with

$$H(s) = \mathcal{L}[h(t)](s) = \int_0^\infty e^{-st} h(t) dt, \quad s \in \mathbb{C}, \quad \text{Re}(s) > 0.$$

In (2.7), $\{Y_n^m\}$ are the spherical harmonics, which are orthonormal as defined in [26], and $\{\hat{U}_n\}/\{\hat{U}_{nm}\}$ are the Fourier/spherical harmonic expansion coefficients of $U|_{r=b}$. Note that the convolution is defined as usual: $(f * g)(t) = \int_0^t f(t - \tau) g(\tau) d\tau$.

Alternatively, we can represent $T_d(U)$ by the temporal convolution in terms of the expansion coefficients of $\partial_t U|_{r=b}$. More precisely, we define

$$\omega_\nu(t) := \omega_\nu(t; d) := -\frac{(d-1)c}{2b} + c \int_0^t \sigma_\nu(\tau) d\tau, \quad (2.9)$$

and note that $\omega'_\nu(t) = c\sigma_\nu(t)$. Then, we find from (2.7) and integration by parts that

$$T_d(U) = -\frac{1}{c} \frac{\partial U}{\partial t} \Big|_{r=b} + \frac{1}{c} \begin{cases} \sum_{|n|=0}^{\infty} \omega_n(t) * \partial_t \widehat{U}_n(b, t) e^{in\phi}, & d = 2, \\ \sum_{n=0}^{\infty} \sum_{|m|=0}^n \omega_{n+1/2}(t) * \partial_t \widehat{U}_{nm}(b, t) Y_n^m(\theta, \phi), & d = 3, \end{cases} \quad (2.10)$$

where for $d = 2, 3$,

$$\omega_\nu(t) = \mathcal{L}^{-1} \left[1 - \frac{(d-2)c}{2bs} + \frac{K'_\nu(sb/c)}{K_\nu(sb/c)} \right] (t), \quad \nu = n, n + 1/2. \quad (2.11)$$

Hereafter, we term σ_ν and ω_ν as the nonreflecting boundary kernels (NRBKs). Since $K_{-n}(z) = K_n(z)$ (see Formula 9.6.6 in [1]), it suffices to consider ω_n and σ_n with $n \geq 0$, for $d = 2$.

Remark 2.1. In the expressions of σ_ν and ω_ν , some terms are added, e.g., s/c and $1/(2b)$ in (2.8), for the purpose of removing the singular part from the ratio K'_ν/K_ν . Indeed, recall the asymptotic formula for fixed $\nu \geq 0$ and large $|z|$ (see Formula 9.7.2 of [1]):

$$K_\nu(z) \sim \sqrt{\frac{\pi}{2z}} e^{-z} \left\{ 1 + \frac{4\nu^2 - 1}{8z} + O(z^{-2}) \right\}, \quad (2.12)$$

for $|\arg z| < 3\pi/2$, and the recurrence relation:

$$zK'_\nu(z) = \nu K_\nu(z) - zK_{\nu+1}(z). \quad (2.13)$$

One verifies that

$$\frac{K'_\nu(z)}{K_\nu(z)} \sim -1 - \frac{1}{2z} + O(z^{-2}). \quad \square \quad (2.14)$$

Remark 2.2. We find that the use of the NRBK ω_ν is more convenient, if one reformulates (2.4) into a first-order (with respect to the time variable) system (cf. [6]), and it is more suitable for analysis as well, while the NRBK σ_ν is more appropriate for computation. \square

We see that NRBCs are global in both time and space. To solve the truncated problem (2.4)-(2.6) efficiently, we need to (i) invert Laplace transform to compute NRBKs; (ii) deal with temporal convolutions efficiently; and (iii) handle the nonlocality of the NRBC in space effectively. The rest of the paper will address these issues.

2.2. Evaluation of the NRBKs. Our starting point is to invert the Laplace transform via evaluating the Bromwich's contour integral:

$$\sigma_\nu(t) = \frac{1}{2\pi i} \int_{\gamma-\infty i}^{\gamma+\infty i} \left(\frac{s}{c} + \frac{1}{2b} + \frac{s K'_\nu(sb/c)}{c K_\nu(sb/c)} \right) e^{ts} ds = \frac{c}{2b^2 \pi i} \int_{\gamma-\infty i}^{\gamma+\infty i} F_\nu(z) e^{czt/b} dz, \quad (2.15)$$

for $\nu = n, n + 1/2$ with $n \geq 0$, where

$$F_\nu(z) = z + \frac{1}{2} + z \frac{K'_\nu(z)}{K_\nu(z)}, \quad (2.16)$$

and γ is the Laplace convergence abscissa, which is a generic constant greater than the real part of any singularity of $F_\nu(z)$.

In order to use the residue theorem to evaluate (2.15), we need to understand the behavior of the poles of $F_\nu(z)$, i.e., the zeros of $K_\nu(z)$.

Lemma 2.1. Let $\nu \geq 0$ be a real number.

- (i) If z is a zero of $K_\nu(z)$, then its complex conjugate \bar{z} is also a zero. Moreover, all complex conjugate pairs of zeros lie in the second and third quadrants with $\text{Re}(z) < 0$.

- (ii) The total number of zeros of $K_\nu(z)$ is the even integer nearest to $\nu - 1/2$, if $\nu - 1/2$ is not an integer, or exactly $\nu - 1/2$, if $\nu - 1/2$ is an integer.
- (iii) All zeros of $K_n(z)$ and $K_{n+1/2}(z)$ are simple, and lie approximately along the left half of the boundary of an eye-shaped domain around $z = 0$ (see Figure 2.1).

Proof. The properties (i) and (ii) can be found from Page 511 of [40]. We now consider the property (iii). As a consequence of (i), it suffices to consider the zeros of $K_\nu(z)$ in the third quadrant and on the negative real axis (i.e., with $-\pi \leq \arg z < -\pi/2$) of the complex plane. According to Formula 9.6.4 of [1], we have the following relation between $K_\nu(z)$ and the Hankel function of the first kind:

$$K_\nu(z) = \frac{\pi i}{2} e^{\frac{1}{2}\nu\pi i} H_\nu^{(1)}(iz), \quad -\pi < \arg z \leq \frac{\pi}{2}, \quad (2.17)$$

which implies that all zeros of $K_\nu(z)$ in the third quadrant (i.e., with $-\pi < \arg z < -\pi/2$) are obtained by rotating all zeros of $H_\nu^{(1)}(z)$ in the fourth quadrant (i.e., with $-\pi/2 < \arg z < 0$) by an angle $-\pi/2$. Recall that the zeros of $H_\nu^{(1)}(z)$ in the fourth quadrant lie approximately along the boundary of an eye-shaped domain around $z = 0$ (see Figure 9.6 and Page 441 of [1]), whose boundary curve intersects the real axis at $z = n$ and the imaginary axis at $z = -ina$, where $a = \sqrt{t_0^2 - 1} \approx 0.66274$ and $t_0 \approx 1.19968$ is the positive root of $\coth t = t$. \square

For clarity, let M_ν be the total number of zeros of $K_\nu(z)$ with $\nu = n, n + 1/2$, that is,

$$M_\nu = \begin{cases} \text{the largest even integer nearest to } n - 1/2, & \text{for } K_n(z), \\ n, & \text{for } K_{n+1/2}(z). \end{cases} \quad (2.18)$$

We plot in Figure 2.1 some samples of zeros of $K_n(z)$ (and $K_{n+1/2}(z)$ for various n , and visualize that for a given n , the zeros sit on the left half boundary of an eye-shaped domain that intersects the imaginary axis approximately at $\pm ni$, and the negative real axis at $-na$ with $a \approx 0.66274$ (see the dashed coordinate grids) as predicted by Lemma 2.1 (iii).

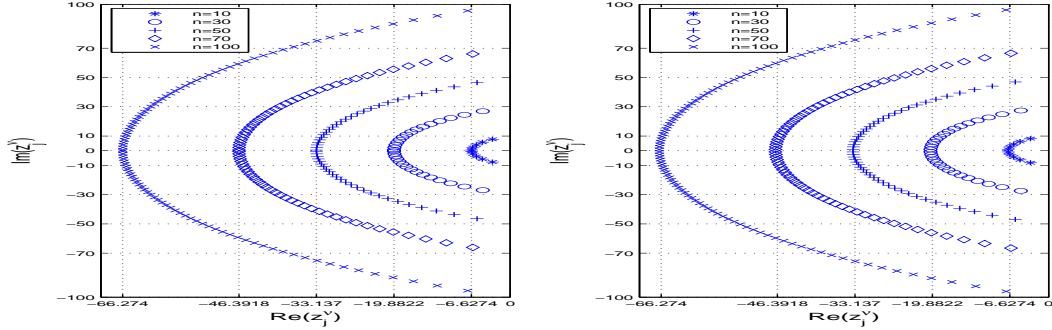


FIGURE 2.1. Distributions of $\{z_j^\nu\}_{j=1}^{M_\nu}$ of K_n (left) and $K_{n+1/2}$ (right) for various n .

With the above understanding of the poles of the integrand $F_\nu(z)$ in (2.16), we now present the exact formula for the NRBKs $\sigma_\nu(t)$ with $\nu = n, n + 1/2$.

Theorem 2.1. Let $\nu = n, n + 1/2$ with $n \geq 0$, and let $\{z_j^\nu\}_{j=1}^{M_\nu}$ be the zeros of $K_\nu(z)$. Then

- for $d = 2$,

$$\sigma_n(t) = \frac{c}{b^2} \left\{ \sum_{j=1}^{M_n} z_j^n e^{ctz_j^n/b} + (-1)^n \int_0^\infty \frac{e^{-ctr/b}}{K_n^2(r) + \pi^2 I_n^2(r)} dr \right\}, \quad (2.19)$$

- for $d = 3$,

$$\sigma_\nu(t) = \frac{c}{b^2} \sum_{j=1}^{M_\nu} z_j^\nu e^{ctz_j^\nu/b}, \quad \nu = n + 1/2, \quad (2.20)$$

where $I_n(z)$ is the modified Bessel function of the first kind (cf. [1]).

We sketch the proof in Appendix A by applying the residue theorem to the Bromwich's contour integral (2.15). We remark that Sofronov [35] derived formulas of similar type by working on much more complicated expressions in terms of Tricomi's confluent hypergeometric functions. However, the formulas in the above theorem are more compact and informative.

Remark 2.3. Based on a delicate study of the logarithmic derivative of the Hankel function $H_\nu^{(1)}(z)$, Alpert et al. [2] (see Theorem 4.1 and Lemma 4.2 in [2]) obtained the following formula:

$$\begin{aligned} z \frac{H_\nu^{(1)'}(z)}{H_\nu^{(1)}(z)} &= iz - \frac{1}{2} + \sum_{j=1}^{N_\nu} \frac{h_{\nu,j}}{z - h_{\nu,j}} \\ &\quad - \frac{1}{\pi i} \int_0^\infty \frac{\pi \cos(\nu\pi)}{\cos^2(\nu\pi) K_\nu^2(r) + (\pi I_\nu(r) + \sin(\nu\pi) K_\nu(r))^2} \frac{1}{ir + z} dr, \end{aligned} \quad (2.21)$$

for any $\nu \neq n + 1/2$, where $h_{\nu,1}, h_{\nu,2}, \dots, h_{\nu,N_\nu}$ are zeros of $H_\nu^{(1)}(z)$, which number N_ν . Interestingly, (2.19) can be derived from (2.21), which is justified in Appendix B. \square

Remark 2.4. Thanks to (2.9), we obtain from Theorem 2.1 the expression of $\omega_\nu(t)$:

- for $d = 2$,

$$\omega_n(t) = -\frac{c}{2b} + \frac{c}{b} \left\{ \sum_{j=1}^{M_n} (e^{ctz_j^n/b} - 1) + (-1)^n \int_0^\infty \frac{1 - e^{-ctr/b}}{r \{K_n^2(r) + \pi^2 I_n^2(r)\}} dr \right\}, \quad (2.22)$$

- for $d = 3$,

$$\omega_\nu(t) = -\frac{c}{b} + \frac{c}{b} \sum_{j=1}^{M_\nu} (e^{ctz_j^\nu/b} - 1), \quad \nu = n + 1/2. \quad \square \quad (2.23)$$

2.3. Computation of the improper integral in (2.19). The computation of the two-dimensional NRBK requires to evaluate the improper integral involving the kernel function:

$$W_n(r) := \frac{1}{K_n^2(r) + \pi^2 I_n^2(r)} := \frac{1}{G_n(r)}, \quad n \geq 0, \quad r > 0, \quad (2.24)$$

whose important properties are characterized below.

Lemma 2.2. For any $n \geq 0$ and any real $r > 0$, we have

- $G_n(r)$ is a convex function of r , and $W_n(r)$ attains its maximum at a unique point.
- For large n , we have the uniform asymptotic estimate:

$$W_n(n\kappa) \sim \frac{n\sqrt{1+\kappa^2}}{\pi} \operatorname{sech}(2n\Theta) := \widetilde{W}_n(n\kappa), \quad (2.25)$$

for $\kappa > 0$, where

$$\Theta = \Theta(\kappa) := \sqrt{1+\kappa^2} + \ln \frac{\kappa}{1+\sqrt{1+\kappa^2}}. \quad (2.26)$$

Approximately, the maximum value of $W_n(r)$ attains at $r = na$ with $a \approx 0.66274$ being the root of Θ , and the maximum value is approximately $n\sqrt{1+a^2}/\pi \approx 0.38187n$.

Proof. (i). We find from Page 374 of [1] that for a given n , $K_n(r), I_n(r) > 0$, and $K_n(r)$ (resp. $I_n(r)$) is monotonically descending (resp. ascending) with respect to r . From the series representation (see Formula 9.6.10 of [1]):

$$I_n(r) = \frac{r^n}{2^n} \sum_{k=0}^{\infty} \frac{r^{2k}}{2^{2k} k! (n+k)!}, \quad n \geq 0,$$

we conclude that $I_n''(r) > 0$. Moreover, since $K_n(r)$ satisfies (see Formula 9.6.1 of [1])

$$r^2 K_n''(r) + r K_n'(r) - (r^2 + n^2) K_n(r) = 0,$$

we have $K_n''(r) > 0$. Therefore, a direct calculation shows that $G_n''(r) > 0$, so $G_n(r)$ is convex.

One verifies that $G_n(0+) = G_n(+\infty) = +\infty$ for all n , which follows from (2.12), and the asymptotic properties (see [1] again):

$$K_\nu(r) \sim \begin{cases} -\ln r, & \text{if } \nu = 0, \\ \frac{\Gamma(\nu)}{2} \left(\frac{r}{2}\right)^{-\nu}, & \text{if } \nu > 0, \end{cases} \quad I_\nu(r) \sim \frac{1}{\Gamma(\nu+1)} \left(\frac{r}{2}\right)^\nu, \quad \nu \geq 0, \quad (2.27)$$

for $0 < r \ll 1$, and

$$I_\nu(r) \sim \sqrt{\frac{1}{2\pi r}} e^r, \quad r \gg 1, \quad \nu \geq 0. \quad (2.28)$$

Since $G_n(r)$ is convex, $G_n(r)$ attains its minimum at a unique point r_0 . Thanks to $G_n'(r) = -W_n'(r)/W_n^2(r)$, $W_n(r)$ has a unique maximum at the same point r_0 .

(ii). Recall that for large n (see Formulas (9.7.7)-(9.7.11) of [1]):

$$\begin{aligned} K_n(n\kappa) &\sim \sqrt{\frac{\pi}{2n}} \frac{e^{-n\Theta}}{(1+\kappa^2)^{1/4}}, & I_n(n\kappa) &\sim \frac{1}{\sqrt{2\pi n}} \frac{e^{n\Theta}}{(1+\kappa^2)^{1/4}}, \\ K_n'(n\kappa) &\sim -\sqrt{\frac{\pi}{2n}} \frac{(1+\kappa^2)^{1/4}}{\kappa} e^{-n\Theta}, & I_n'(n\kappa) &\sim \frac{1}{\sqrt{2\pi n}} \frac{(1+\kappa^2)^{1/4}}{\kappa} e^{n\Theta}, \end{aligned} \quad (2.29)$$

which, together with (2.24), leads to the asymptotic estimate (2.25). Thus, the maximum value of $W_n(r)$ approximately attains at the unique root of $\Theta(\kappa)$, which turns out to be $a \approx 0.66274$ as in Figure 2.1, and the maximum value is about $n\sqrt{1+a^2}/\pi \approx 0.38187n$. \square

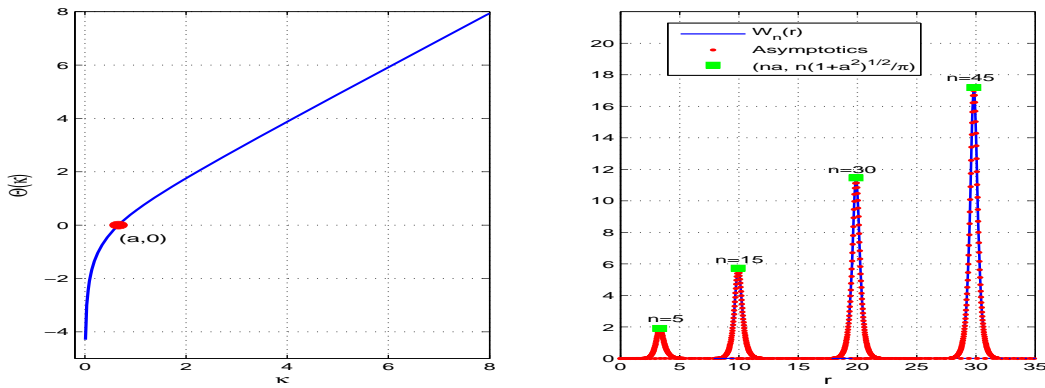


FIGURE 2.2. Left: graph of $\Theta(\kappa), \kappa \in (0, 8]$ defined in (2.26). Right: W_n against the asymptotic estimate \tilde{W}_n (“•”) for samples of $n = 5, 15, 30, 45$.

We depict in Figure 2.2 (left) the graph of $\Theta(\kappa)$, and highlight the zero point $(a, 0)$. Observe that $\Theta(\kappa)$ grows like κ , when $\kappa > a$. We also plot in Figure 2.2 (right) several sample graphs of

W_n (solid lines) and the asymptotic estimate \widetilde{W}_n (“•”) for $n = 5, 15, 30, 45$, and particularly mark the asymptotic point $(na, n\sqrt{1+a^2}/\pi)$ of the maximum of $W_n(r)$ obtained in Lemma 2.2 (ii). Observe that even for small n , the asymptotic estimate provides a very accurate approximation of W_n . These properties greatly facilitate the computation of the improper integral. Indeed, we can truncate $(0, \infty)$ to a narrow interval (of length about 20 for $n \geq 5$ in our numerical computations in Section 5) around the point $r = na$.

2.4. Rapid evaluation of the temporal convolution. Remarkably, the presence of the time variable t in the exponentials in (2.19) and (2.20) allows us to eliminate the burden of history dependence of the temporal convolution easily. More precisely, given a function $g(t)$, we define

$$f(t; r) := e^{-ctr/b} * g(t) = \int_0^t e^{-c(t-\tau)r/b} g(\tau) d\tau.$$

One verifies readily that

$$f(t + \Delta t; r) = e^{-c\Delta t r/b} f(t; r) + \int_t^{t+\Delta t} e^{-c(t+\Delta t-\tau)r/b} g(\tau) d\tau, \quad (2.30)$$

so $f(t; r)$ can march in t with step size Δt recursively. This enables us to compute the time convolution rapidly. For example, in the 2-D case,

$$\begin{aligned} [\sigma_n * g](t) &= \int_0^t \sigma_n(t-\tau) g(\tau) d\tau = \frac{c}{b^2} \sum_{j=1}^{M_n} z_j^n \int_0^t e^{c(t-\tau)z_j^n/b} g(\tau) d\tau \\ &\quad + \frac{(-1)^n c}{b^2} \int_0^\infty \frac{1}{K_n^2(r) + \pi^2 I_n^2(r)} \left[\int_0^t e^{-c(t-\tau)r/b} g(\tau) d\tau \right] dr \\ &= \frac{c}{b^2} \sum_{j=1}^{M_n} z_j^n f(t; -z_j^n) + \frac{(-1)^n c}{b^2} \int_0^{+\infty} f(t; r) W_n(r) dr. \end{aligned} \quad (2.31)$$

Thanks to (2.30), $[\sigma_n * g](t + \Delta t)$ can be computed recursively from the previous step and the history dependence is then narrowed down to $[t, t + \Delta t]$. We also refer to Subsection 4.4 for more detailed discussions.

3. A PRIORI ESTIMATES

In this section, we analyze the well-posedness of the truncated problem (2.4)-(2.6), and provide *a priori* estimates for its solution.

We first recall the Plancherel or Parseval results for the Laplace transform.

Lemma 3.1. *Let $s = s_1 + is_2$ with $s_1, s_2 \in \mathbb{R}$. If f, g are Laplace transformable, then*

$$\frac{1}{2\pi} \int_{-\infty}^{+\infty} \mathcal{L}[f](s) \mathcal{L}[\bar{g}](s) ds_2 = \int_0^{+\infty} e^{-2s_1 t} f(t) \bar{g}(t) dt, \quad \forall s_1 > \gamma, \quad (3.1)$$

where γ is the abscissa of convergence for both f and g , and \bar{g} is the complex conjugate of g .

Proof. This identity can be proved by following the same lines as for (2.46) in [8] (or [11]). \square

For notational convenience, we introduce the modified spherical Bessel function (cf. [40]):

$$k_n(z) = \sqrt{\frac{2}{\pi z}} K_{n+1/2}(z) \Rightarrow \frac{k'_n(z)}{k_n(z)} = -\frac{1}{2z} + \frac{K'_{n+1/2}(z)}{K_{n+1/2}(z)}, \quad (3.2)$$

and by (2.11),

$$\omega_{n+1/2}(t) = \mathcal{L}^{-1} \left[1 + \frac{k'_n(sb/c)}{k_n(sb/c)} \right] (t), \quad n \geq 0. \quad (3.3)$$

The following properties are also indispensable for the analysis.

Lemma 3.2. *Let $s = s_1 + is_2$ with $s_1, s_2 \in \mathbb{R}$. Then for any $s_1 > 0$,*

$$(i) \operatorname{Re}\left(s \frac{Z'_n(sb/c)}{Z_n(sb/c)}\right) \leq 0, \quad \operatorname{Re}\left(\frac{Z'_n(sb/c)}{Z_n(sb/c)}\right) \leq 0; \quad (ii) \operatorname{Im}\left(s \frac{Z'_n(sb/c)}{Z_n(sb/c)}\right) \leq 0, \quad \forall s_2 \geq 0, \quad (3.4)$$

where $Z_n(z) = K_n(z)$ or $k_n(z)$.

Proof. The results with $Z_n = K_n$ were proved in Chen [6]. We next prove (3.4) with $Z_n = k_n$ by using a similar argument. By applying Laplace transform to (2.1)-(2.3), exterior to $D = B$ with $F = U_0 = U_1 \equiv 0$ and $G = U|_{r=b}$, and denoting $u = \mathcal{L}[U]$, we obtain

$$\begin{aligned} -c^2 \Delta u + s^2 u &= 0, \quad \text{in } \Omega_{\text{ext}} = \mathbb{R}^d \setminus \bar{B}, \quad s \in \mathbb{C}, \quad \operatorname{Re}(s) > 0; \\ u|_{r=b} &= \psi = \mathcal{L}[U|_{r=b}]; \quad c \partial_r u + su = o(r^{(1-d)/2}), \quad d = 2, 3, \end{aligned} \quad (3.5)$$

which admits the series solution

$$u(r, \theta, \phi, s) = \sum_{n=0}^{\infty} \frac{k_n(sr/c)}{k_n(sb/c)} \sum_{|m|=0}^n \hat{\psi}_{nm}(s) Y_n^m(\theta, \phi), \quad (3.6)$$

where $\{\hat{\psi}_{nm}\}$ are the spherical harmonic expansion coefficients of ψ . Multiplying the first equation of (3.5) by \bar{u} and integrating over $\Omega_{b,\rho} := B_\rho \setminus \bar{B}$, where B_ρ is a ball of radius $\rho > b$, the imaginary part of the resulting equation reads

$$2s_1 s_2 \int_{\Omega_{b,\rho}} |u|^2 d\mathbf{x} - c^2 \operatorname{Im} \int_{\partial\Omega_{b,\rho}} \frac{\partial u}{\partial \mathbf{n}} \bar{u} d\gamma = 0, \quad (3.7)$$

where \mathbf{n} is the unit outer normal of $\partial\Omega_{b,\rho}$.

Since $s_1 > 0$, multiplying (3.7) by s_2 yields

$$s_2 \operatorname{Im} \int_{\{r=b\}} \frac{\partial u}{\partial r} \bar{u} d\gamma \leq s_2 \operatorname{Im} \int_{\{r=\rho\}} \frac{\partial u}{\partial r} \bar{u} d\gamma. \quad (3.8)$$

It is clear that $u = k_n(sr/c)/k_n(sb/c) \hat{\psi}_{nm}(s) Y_n^m(\theta, \phi)$ is a solution of (3.5), so using the orthogonality of $\{Y_n^m\}$, we obtain from (3.8) that

$$\frac{b}{c} \operatorname{Im}\left(s_2 s \frac{k'_n(sb/c)}{k_n(sb/c)}\right) |\hat{\psi}_{nm}|^2 \leq \frac{\rho}{c} \operatorname{Im}\left(s_2 s \frac{k'_n(s\rho/c)}{k_n(s\rho/c)}\right) |\hat{\psi}_{nm}|^2. \quad (3.9)$$

We find from (2.12) and (3.2) that $k'_n(s\rho/c)$ decays exponentially if $s_1 > 0$, so the right hand side of (3.8) tends to zero as $\rho \rightarrow +\infty$. Thus, letting $\rho \rightarrow +\infty$ in (3.9) leads to

$$\operatorname{Im}\left(s_2 s \frac{k'_n(sb/c)}{k_n(sb/c)}\right) \leq 0. \quad (3.10)$$

If $s_2 \geq 0$, we obtain (ii) in (3.4). Next, we prove the first inequality of (i) in (3.4). Recall the formula (see Lemma 2.3 of [6]):

$$|K_{n+1/2}(sr)|^2 = \frac{1}{2} \int_0^{+\infty} e^{-\frac{|s|^2 r^2}{2r} - \frac{s^2 + \bar{s}^2}{2|s|^2} \tau} K_{n+1/2}(\tau) \frac{d\tau}{\tau}, \quad s_1 > 0,$$

which implies that $|K_{n+1/2}(sr)|^2$ is monotonically descending with respect to r . The property $\frac{d}{dr} |K_{n+1/2}(sr)|^2 \leq 0$, together with (3.2), implies $\operatorname{Re}\left(s \frac{k'_n(sb/c)}{k_n(sb/c)}\right) \leq 0$. Denoting $s \frac{k'_n(sb/c)}{k_n(sb/c)} = \gamma_1 + i\gamma_2$ with $\gamma_1, \gamma_2 \in \mathbb{R}$, we know from (3.10) that $\gamma_1 \leq 0$ and $s_2 \gamma_2 \leq 0$. Therefore,

$$\operatorname{Re}\left(\frac{k'_n(sb/c)}{k_n(sb/c)}\right) = \operatorname{Re}\left(\frac{\gamma_1 + i\gamma_2}{s}\right) = \frac{1}{|s|^2} (s_1 \gamma_1 + s_2 \gamma_2) \leq 0.$$

This ends the proof. \square

With the above preparations, we can derive the following important property.

Theorem 3.1. *For any $v \in L^2(0, T)$, we have*

$$\int_0^T [\omega_\nu * v](t) \bar{v}(t) dt \leq \int_0^T |v(t)|^2 dt, \quad \forall T > 0, \quad n \geq 0, \quad (3.11)$$

where ω_ν is the NRBK given by (2.11) (or (3.3) for $d = 3$).

Proof. Let $\tilde{v} = v \mathbf{1}_{[0, T]}$, where $\mathbf{1}_{[0, T]}$ is the characteristic function of $[0, T]$. Then we obtain from (3.1) that for $d = 3$,

$$\begin{aligned} \int_0^T e^{-2s_1 t} [\omega_{n+1/2} * v](t) \bar{v}(t) dt &= \int_0^{+\infty} e^{-2s_1 t} [\omega_{n+1/2} * \tilde{v}](t) \bar{\tilde{v}}(t) dt \\ &= \frac{1}{2\pi} \int_{-\infty}^{+\infty} \left[\frac{k'_n(sb/c)}{k_n(sb/c)} + 1 \right] |\mathcal{L}[\tilde{v}](s)|^2 ds_2 \\ &= \frac{1}{2\pi} \int_{-\infty}^{+\infty} \frac{k'_n(sb/c)}{k_n(sb/c)} |\mathcal{L}[\tilde{v}](s)|^2 ds_2 + \frac{1}{2\pi} \int_{-\infty}^{+\infty} |\mathcal{L}[\tilde{v}](s)|^2 ds_2. \end{aligned}$$

It is clear that by (3.1) with $f = g = \tilde{v}$,

$$\frac{1}{2\pi} \int_{-\infty}^{+\infty} |\mathcal{L}[\tilde{v}](s)|^2 ds_2 = \int_0^{+\infty} e^{-2s_1 t} |\tilde{v}(t)|^2 dt = \int_0^T e^{-2s_1 t} |v(t)|^2 dt.$$

Using (2.13) and the properties $\overline{K_\nu(z)} = K_\nu(\bar{z})$ and $\mathcal{L}[\tilde{v}](\bar{s}) = \overline{\mathcal{L}[\tilde{v}](s)}$, we find

$$\begin{aligned} \frac{1}{2\pi} \int_{-\infty}^{+\infty} \frac{k'_n(sb/c)}{k_n(sb/c)} |\mathcal{L}[\tilde{v}](s)|^2 ds_2 &= \frac{1}{\pi} \int_0^{+\infty} \operatorname{Re} \left(\frac{k'_n(sb/c)}{k_n(sb/c)} \right) |\mathcal{L}[\tilde{v}](s)|^2 ds_2 \\ &= \frac{1}{\pi} \int_0^{+\infty} \operatorname{Re} \left(\frac{k'_n(sb/c)}{k_n(sb/c)} \right) |s|^2 \left| \mathcal{L} \left[\int_0^t \tilde{v}(\tau) d\tau \right](s) \right|^2 ds_2. \end{aligned} \quad (3.12)$$

Thus, we conclude from Lemma 3.2 and the above identities that for $s_1 > 0$,

$$\int_0^T e^{-2s_1 t} [\omega_{n+1/2} * v](t) \bar{v}(t) dt \leq \int_0^T e^{-2s_1 t} |v(t)|^2 dt. \quad (3.13)$$

Notice that the asymptotic formulas in (2.27) are also valid for complex r (see Formula 9.6.9 of [1]), which, together with Lemma 2.1, implies that $k'_n(sb/c)/k_n(sb/c)$ is analytic for all $\operatorname{Re}(s) \geq 0$ but $|s| \neq 0$, and $\lim_{s_1 \rightarrow 0^+} |s|^2 k'_n(sb/c)/k_n(sb/c)$ exists for all $s_2 \geq 0$. Hence, the integral in (3.12) is finite. By letting $s_1 \rightarrow 0^+$ in (3.13) leads to the desired result for $d = 3$.

The result (3.11) with $d = 2$ can be proved in a similar fashion. \square

Corollary 3.1. *Suppose that $v' \in L^2(0, T)$ with $v(0) = 0$. Then we have*

$$\int_0^T [\sigma_\nu * v](t) \bar{v}'(t) dt \leq \frac{1}{c} \int_0^T |v'(t)|^2 dt + \frac{d-1}{4b} |v(T)|^2, \quad \forall T > 0, \quad (3.14)$$

for $\nu = n, n+1/2$, where $\sigma_\nu(t)$ is the NRBK defined in (2.8).

Proof. By (2.9), we have $\omega'_\nu(t) = c\sigma_\nu(t)$, $\omega_\nu(0) = -\frac{(d-1)c}{2b}$. Thus, we obtain from integration by parts and the fact $v(0) = 0$ that

$$[\omega_\nu * v'](t) = -\frac{(d-1)c}{2b} v(t) + c[\sigma_\nu * v](t).$$

By Theorem 3.1 with v' in place of v ,

$$\begin{aligned} \int_0^T [\omega_\nu * v'](t) \bar{v}'(t) dt &= -\frac{(d-1)c}{2b} \int_0^T v(t) \bar{v}'(t) dt + c \int_0^T [\sigma_\nu * v](t) \bar{v}'(t) dt \\ &= -\frac{(d-1)c}{4b} |v(T)|^2 + c \int_0^T [\sigma_\nu * v](t) \bar{v}'(t) dt \leq \int_0^T |v'(t)|^2 dt. \end{aligned}$$

This gives (3.14). \square

Now, we are ready to analyze the stability of the solution of the truncated problem (2.4)-(2.6). To this end, we assume that the scatter D is a simply connected domain with Lipschitz boundary Γ_D , and the Dirichlet data $G = 0$ on Γ_D . Denote $X := \{U \in H^1(\Omega) : U|_{\Gamma_D} = 0\}$, and let $(\cdot, \cdot)_{L^2(\Omega)}$ and $\|\cdot\|_{L^2(\Omega)}$ be the inner product and norm of $L^2(\Omega)$, respectively.

Theorem 3.2. *Let $U \in X$ be the solution of (2.4)-(2.6) with $G = 0$. If $U_0 \in H^1(\Omega)$, $U_1 \in L^2(\Omega)$ and $F \in L^1(0, T; L^2(\Omega))$ for any $T > 0$, then we have $\nabla U \in L^\infty(0, T; (H^1(\Omega))^d)$, $\partial_t U \in L^\infty(0, T; L^2(\Omega))$, and there holds*

$$\begin{aligned} \|\partial_t U\|_{L^\infty(0, T; L^2(\Omega))} + c \|\nabla U\|_{L^\infty(0, T; L^2(\Omega))} \\ \leq C (\|U_1\|_{L^2(\Omega)} + c \|\nabla U_0\|_{L^2(\Omega)} + \|F\|_{L^1(0, T; L^2(\Omega))}), \end{aligned} \quad (3.15)$$

where C is a positive constant independent of any functions and c, b . Moreover, if the source term $F \equiv 0$, we have the conservation of the energy: $E'(t) = 0$ for all $t \geq 0$, where

$$E(t) = \int_\Omega (|\partial_t U|^2 + c^2 |\nabla U|^2) d\mathbf{x} - 2c^2 \int_0^t \int_{\Gamma_b} T_d(U) \partial_\tau \bar{U} d\gamma d\tau. \quad (3.16)$$

Proof. Multiplying (2.4) by $2\partial_t \bar{U}$ and integrating over Ω , we derive from the Green's formula that for any $t > 0$,

$$\frac{d}{dt} \left(\|\partial_t U\|_{L^2(\Omega)}^2 + c^2 \|\nabla U\|_{L^2(\Omega)}^2 \right) - 2c^2 \int_{\Gamma_b} T_d(U) \partial_t \bar{U} d\gamma = 2(F, \partial_t U)_{L^2(\Omega)}. \quad (3.17)$$

Integrating the above equation over $(0, t)$, we find that for any $t > 0$,

$$\begin{aligned} \|\partial_t U\|_{L^2(\Omega)}^2 + c^2 \|\nabla U\|_{L^2(\Omega)}^2 - 2c^2 \int_0^t \int_{\Gamma_b} T_d(U) \partial_\tau \bar{U} d\gamma d\tau \\ = 2 \int_0^t (F, \partial_\tau U)_{L^2(\Omega)} d\tau + \|U_1\|_{L^2(\Omega)}^2 + c^2 \|\nabla U_0\|_{L^2(\Omega)}^2 \\ \leq 2 \|\partial_t U\|_{L^\infty(0, T; L^2(\Omega))} \|F\|_{L^1(0, T; L^2(\Omega))} + \|U_1\|_{L^2(\Omega)}^2 + c^2 \|\nabla U_0\|_{L^2(\Omega)}^2. \end{aligned} \quad (3.18)$$

We next show that for any $t > 0$,

$$\int_0^t \int_{\Gamma_b} T_d(U) \partial_\tau \bar{U} d\gamma d\tau \leq 0. \quad (3.19)$$

For $d = 3$, it follows from (2.10), Theorem 3.1 and the orthogonality of $\{Y_n^m\}$ that

$$\begin{aligned} \int_0^t \int_{\Gamma_b} T_d(U) \partial_\tau \bar{U} d\gamma d\tau &= -\frac{1}{c} \int_0^t \|\partial_\tau U\|_{L^2(\Gamma_b)}^2 d\tau \\ &\quad + \frac{1}{c} \sum_{n=0}^{\infty} \sum_{|m|=0}^n \int_0^t [\omega_{n+1/2} * \partial_\tau \hat{U}_{nm}(b, \tau)] \partial_\tau \bar{\hat{U}}_{nm}(b, \tau) d\tau \\ &\stackrel{(3.11)}{\leq} -\frac{1}{c} \int_0^t \|\partial_\tau U\|_{L^2(\Gamma_b)}^2 d\tau + \frac{1}{c} \sum_{n=0}^{\infty} \sum_{|m|=0}^n \int_0^t |\partial_\tau \hat{U}_{nm}(b, \tau)|^2 d\tau = 0. \end{aligned}$$

This verifies (3.19) with $d = 3$. Similarly, one can justify (3.19) with $d = 2$. Consequently, the estimate (3.15) follows from (3.18), (3.19) and the Cauchy-Schwarz inequality.

Letting $F \equiv 0$ in (3.18) leads to the conservation of energy. \square

Remark 3.1. Note that (i) if $T_d(U)$ is given by (2.7), we can use Corollary 3.1 to verify (3.19), and (ii) a similar estimate for $d = 2$ was derived by [6] with a slightly different argument. \square

4. SPECTRAL-GALERKIN APPROXIMATION AND NEWMARK'S TIME INTEGRATION

This section is devoted to numerical approximation of the truncated problem (2.4)-(2.6) with a focus on the treatment for the NRBC (2.6). Note that if the scatter D is a disk/ball (i.e., Ω in (2.4)-(2.6) is an annulus/spherical shell), the nonlocality of the NRBC in space becomes local in the space of Fourier/spherical harmonic coefficients in polar/spherical coordinates. Correspondingly, the truncated problem can be reduced to a sequence of one-dimensional problems with mixed boundary conditions at the outer artificial boundary. In order to deal with a general scatter, one may resort to the transformed field expansion method (TFE) (cf. [28]), which has been successfully applied to time-harmonic Helmholtz equations (cf. [29, 13, 30]). The use of this method allows us to solve a sequence of truncated problems (2.4)-(2.6) in regular domains. Accordingly, it is essential to construct a fast and accurate solver for (2.4)-(2.6) in an annulus or a spherical shell, which will be the concern of this section. We shall report the combination of the solver with the TFE method in a future work as the implementation is rather involved.

4.1. Notion of TFE. We outline the TFE method for (2.4)-(2.6) with $d = 2$ and

$$\Gamma_D = \{r = b_0 + \eta(\phi) : 0 \leq \phi < 2\pi\}, \quad b > b_0 + \max_{\phi \in [0, 2\pi]} |\eta(\phi)|,$$

where $r(\phi) = b_0 + \eta(\phi)$ is the parametric equation of the boundary of the scatter D .

- Make a change of variables

$$r' = \frac{(b - b_0)r - b\eta(\phi)}{(b - b_0) - \eta(\phi)}, \quad \phi' = \phi,$$

which maps Ω to the annulus $\Omega_0 = \{(r', \phi') : b_0 < r' < b, 0 \leq \phi' < 2\pi\}$. To simplify the notation, we still use U, F, r, ϕ etc. to denote the transformed functions or variables. Then the problem (2.4)-(2.6) becomes

$$\begin{aligned} \partial_t^2 U &= c^2 \Delta U + F + J(\eta, U), \quad \text{in } \Omega_0, \quad t > 0; \\ U &= U_0, \quad \partial_t U = U_1, \quad \text{in } \Omega_0, \quad t = 0; \\ U|_{r=b_0} &= G, \quad t > 0; \quad (\partial_r U - T_d(U))|_{r=b} = L(\eta, U)|_{r=b}, \quad t > 0, \end{aligned}$$

where $J(\eta, U)$ and $L(\eta, U)$ contain differential operators with nonconstant coefficients.

- To solve the transformed problem efficiently, we adopt the boundary perturbation technique by viewing the obstacle as a perturbation of the disk. More precisely, we write $\eta = \varepsilon \zeta$ and expand the solution U as $U(r, \phi, t; \varepsilon) = \sum_{l=0}^{\infty} U_l(r, \phi, t) \varepsilon^l$, and likewise for the data. Formally, we obtain the sequence of equations after collecting the terms of ε^l (see [29]):

$$\begin{aligned} \partial_t^2 U_l &= c^2 \Delta U_l + F_l + \tilde{J}(\eta, U_{l-4}, \dots, U_{l-1}), \quad \text{in } \Omega_0, \quad t > 0; \\ U_l &= U_{0,l}, \quad \partial_t U_l = U_{1,l}, \quad \text{in } \Omega_0, \quad t = 0; \\ U_l|_{r=b_0} &= G_l, \quad t > 0; \quad (\partial_r U_l - T_d(U_l))|_{r=b} = \tilde{L}(\eta, U_{l-1})|_{r=b}, \quad t > 0. \end{aligned}$$

- Solve the above equation for $l = 0, 1, \dots$, and sum up the series by using a Padé approximation.

4.2. Prototype equation and dimension reduction. Under this notion, the whole algorithm boils down to solving a sequence of prototype equations. More precisely, we consider

$$\begin{aligned} \partial_t^2 U &= c^2 \Delta U + F, \quad \text{in } \Omega_0 = \{\mathbf{x} \in \mathbb{R}^d : b_0 < |\mathbf{x}| < b\}, \quad t > 0; \\ U &= U_0, \quad \partial_t U = U_1, \quad \text{in } \Omega_0, \quad t = 0; \quad U|_{r=b_0} = 0, \quad (\partial_r U - T_d(U))|_{r=b} = 0, \quad t > 0, \end{aligned} \quad (4.20)$$

where $T_d(U)$ is the DtN map as before. We expand the solution and given data in Fourier series/spherical harmonic series. Then the problem (4.20), after a polar (in 2-D) and spherical (in 3-D) transform, reduces to a sequence of one-dimensional problems (for brevity, we use u to denote the Fourier/spherical harmonic expansion coefficients of U , and likewise, we use u_0, u_1 and f to denote the expansion coefficients of U_0, U_1 and F , respectively):

$$\begin{aligned} \frac{\partial^2 u}{\partial t^2} - \frac{c^2}{r^{d-1}} \frac{\partial}{\partial r} \left(r^{d-1} \frac{\partial u}{\partial r} \right) + c^2 \beta_n \frac{u}{r^2} &= f, \quad b_0 < r < b, \quad t > 0; \\ u|_{t=0} &= u_0, \quad \frac{\partial u}{\partial t} \Big|_{t=0} = u_1, \quad b_0 < r < b; \quad u|_{r=b_0} = 0, \quad t > 0; \\ \left(\frac{1}{c} \frac{\partial u}{\partial t} + \frac{\partial u}{\partial r} + \frac{d-1}{2r} u \right) \Big|_{r=b} &= \int_0^t \sigma_\nu(t-\tau) u(b, \tau) d\tau, \quad t > 0, \end{aligned} \quad (4.21)$$

where $\beta_n = n^2, n(n+1)$ and $\nu = n, n+1/2$ for $d = 2, 3$, respectively.

Since σ_ν is real, the real and imaginary parts of u and the given data can be decoupled. In what follows, we assume they are real.

4.3. Spectral-Galerkin approximation in space. We apply the Legendre spectral Galerkin method to approximate (4.21) in space. For convenience of implementation, we transform the interval (b_0, b) to the reference interval $I = (-1, 1)$ by $r = \frac{b-b_0}{2}x + \frac{b+b_0}{2}$ with $x \in \bar{I}$, and denote the transformed functions by $v(x, t) = u(r, t)$, $h(x, t) = f(r, t)$ and $v_i(x) = u_i(r)$ with $i = 0, 1$, respectively. Then (4.21) can be reformulated as

$$\begin{aligned} \frac{\partial^2 v}{\partial t^2} - \frac{\tilde{c}^2}{(x+c_0)^{d-1}} \frac{\partial}{\partial x} \left((x+c_0)^{d-1} \frac{\partial v}{\partial x} \right) + \tilde{c}^2 \beta_n \frac{v}{(x+c_0)^2} &= h, \quad x \in I, \quad t > 0; \\ v(x, 0) &= v_0(x), \quad \frac{\partial v}{\partial t}(x, 0) = v_1(x), \quad x \in I; \quad v(-1, t) = 0, \quad t > 0; \\ \left(\frac{1}{c} \frac{\partial v}{\partial t} + \frac{2}{b-b_0} \frac{\partial v}{\partial x} + \frac{d-1}{2b} v \right) (1, t) &= \int_0^t \sigma_\nu(t-\tau) v(1, \tau) d\tau, \quad t > 0, \end{aligned} \quad (4.22)$$

where the constants $\tilde{c} = \frac{2c}{b-b_0}$ and $c_0 = \frac{b+b_0}{b-b_0}$.

Let $V_N := \{\psi \in P_N : \psi(-1) = 0\}$, where P_N is the set of all algebraic polynomials of degree at most N . The semi-discretization Legendre spectral-Galerkin approximation of (4.22) is to find $v_N(x, t) \in V_N$ for all $t > 0$ such that for all $w \in V_N$,

$$\begin{aligned} (\ddot{v}_N, w)_\varpi + \tilde{c}(1+c_0)^{d-1} \dot{v}_N(1, t) w(1) + \tilde{c}^2 (\partial_x v_N, \partial_x w)_\varpi + \tilde{c}^2 \beta_n (v_N(x+c_0)^{-2}, w)_\varpi \\ + \frac{2c^2}{b-b_0} (1+c_0)^{d-1} \left(\frac{d-1}{2b} v_N(1, t) - \sigma_\nu(t) * v_N(1, t) \right) w(1) &= (I_N h, w)_\varpi, \\ v_N(x, 0) &= v_{0,N}(x), \quad \dot{v}_N(x, 0) = v_{1,N}(x), \quad x \in I, \end{aligned} \quad (4.23)$$

where $(\cdot, \cdot)_\varpi$ is the (weighted) inner product of $L_\varpi^2(I)$ with the weight function $\varpi = (x+c_0)^{d-1}$, \ddot{v} denotes $\partial_t^2 v$ or $\frac{d^2 v}{dt^2}$ as usual, I_N is the interpolation operator on $(N+1)$ Legendre-Gauss-Lobatto points, and $v_{0,N}, v_{1,N} \in P_N$ are suitable approximations of the initial values.

Like Theorem 3.2, we have the following *a priori* estimates.

Theorem 4.1. *Let v_N be the solution of (4.23). Then for all $t > 0$,*

$$\begin{aligned} & \|\partial_t v_N\|_{L^2_\infty(I)}^2 + \tilde{c}^2 (\|\partial_x v_N\|_{L^2_\infty(I)}^2 + \beta_n \|v_N/(x+c_0)\|_{L^2_\infty(I)}^2) \\ & \leq C \left(\|v_{1,N}\|_{L^2_\infty(I)}^2 + \tilde{c}^2 (\|\partial_x v_{0,N}\|_{L^2_\infty(I)}^2 + \beta_n \|v_{0,N}/(x+c_0)\|_{L^2_\infty(I)}^2) + \|I_N h\|_{L^2_\infty(I)}^2 \right), \end{aligned} \quad (4.24)$$

where C is a positive constant independent of N, \tilde{c} and b .

This estimate holds for (4.22) with v, v_0, v_1, h in place of $v_N, v_{0,N}, v_{1,N}, I_N h$, respectively.

Proof. Taking $w = \partial_t v_N$ in (4.23), and integrating the resulted equation with respect to t , we use Corollary 3.1 and the argument similar to that for Theorem 3.2 to derive the estimates. \square

Remark 4.1. *Equipped with Theorem 4.1, we can analyze the convergence of the semi-discretized scheme (4.23) as on Page 341 of [32].* \square

We next examine the linear system of (4.23). As shown in [31, 32], it is advantageous to construct basis functions satisfying the underlying homogeneous Dirichlet boundary conditions. Let $L_l(x)$ be the Legendre polynomial of degree l (see, e.g., [36]), and define $\phi_k(x) = L_k(x) + L_{k+1}(x)$. Then $\phi_k(-1) = 0$ and $V_N = \text{span}\{\phi_k : 0 \leq k \leq N-1\}$. Note that $\phi_k(1) = 2$. Setting

$$v_N(x, t) = \sum_{j=0}^{N-1} \hat{v}_j(t) \phi_j(x), \quad \mathbf{v}(t) = (\hat{v}_0, \dots, \hat{v}_{N-1})^t, \quad m_{ij} = (\phi_j, \phi_i)_\varpi, \quad s_{ij} = (\phi'_j, \phi'_i)_\varpi,$$

we obtain the system:

$$M\ddot{\mathbf{v}} + \alpha E\dot{\mathbf{v}} + \tilde{c}^2(S + \beta_n \widetilde{M})\mathbf{v} + \mu E\mathbf{v} - c\alpha \left(\sigma_\nu * \sum_{j=0}^{N-1} \hat{v}_j \right) \mathbf{1} = \mathbf{h}, \quad (4.25)$$

with $\mathbf{v}(0) = \mathbf{v}_0$ and $\dot{\mathbf{v}}(0) = \mathbf{v}_1$, where $M = (m_{ij}), S = (s_{ij}), \widetilde{M} = (\tilde{m}_{ij})$ and $E = \mathbf{1}\mathbf{1}^t$ is an $N \times N$ matrix of all ones. In (4.25), \mathbf{v}_0 and \mathbf{v}_1 are column- N vectors of the expansion coefficients of $v_{0,N}$ and $v_{1,N}$ in terms of $\{\phi_k\}$, and the constants $\alpha = 8c(1+c_0)^{d-1}/(b-b_0)$ and $\mu = 4c^2(d-1)(1+c_0)^{d-1}/(b(b-b_0))$.

4.4. Newmark's time integration. To discretize the second-order ordinary differential system (4.25), we resort to the implicit second-order Newmark's scheme, which has wide applications in the field of structural mechanics (see [27, 41]). To this end, let Δt be the time-stepping size, and let $\{\mathbf{v}^m, \dot{\mathbf{v}}^m, \ddot{\mathbf{v}}^m\}$ be the approximation of $\{\mathbf{v}, \dot{\mathbf{v}}, \ddot{\mathbf{v}}\}$ at $t = t_m = m\Delta t$, and $\mathbf{h}^m = \mathbf{h}(t_m)$.

We first take care of the convolution term $[\sigma_\nu * \sum_{j=0}^{N-1} \hat{v}_j](t_{m+1})$ in (4.25):

$$\begin{aligned} \left[\sigma_\nu * \sum_{j=0}^{N-1} \hat{v}_j \right](t_{m+1}) &= \sum_{j=0}^{N-1} \int_{t_m}^{t_{m+1}} \sigma_n(t_{m+1} - \tau) \hat{v}_j(\tau) d\tau + \sum_{j=0}^{N-1} \int_0^{t_m} \sigma_n(t_{m+1} - \tau) \hat{v}_j(\tau) d\tau \\ &\approx \frac{\Delta t}{2} \left(\sigma_\nu(0) \sum_{j=0}^{N-1} \hat{v}_j^{m+1} + \sigma_\nu(\Delta t) \sum_{j=0}^{N-1} \hat{v}_j^m \right) + \sum_{j=0}^{N-1} \int_0^{t_m} \sigma_n(t_{m+1} - \tau) \hat{v}_j(\tau) d\tau \\ &\approx \frac{\Delta t}{2} \sigma_\nu(0) E \mathbf{v}^{m+1} + \mathbf{g}^m, \end{aligned}$$

where we used the Trapezoidal rule (of order $O(\Delta t^3)$) to approximate the integral over (t_m, t_{m+1}) , and denoted by \mathbf{g}^m the approximation of the remaining terms. Note that \mathbf{g}^m depends on the history $\mathbf{v}^l (0 \leq l \leq m)$, but fortunately, it can be evaluated recursively and rapidly as described in Subsection 2.4. Moreover, only the history data $\sum \hat{v}_j^l (0 \leq l \leq m)$ need to be stored, and no any matrix-vector multiplication is involved. As a result, the burden of the history dependence can be eliminated.

Denoting

$$A = M, \quad B = \alpha E, \quad C = \tilde{c}^2(S + \beta_n \widetilde{M}) + \left(\mu - c\alpha \frac{\Delta t}{2} \sigma_\nu(0)\right) E, \quad (4.26)$$

and $\mathbf{f}^{m+1} = \mathbf{h}^{m+1} + c\alpha \mathbf{g}^m$, we carry out the full scheme for (4.22) as follows.

- (i) Set $\mathbf{v}^0 = \mathbf{v}_0$ and $\dot{\mathbf{v}}^0 = \mathbf{v}_1$, and compute $\ddot{\mathbf{v}}^0$ from the system (4.25) by

$$\ddot{\mathbf{v}}^0 = M^{-1}\{\mathbf{h}^0 - \alpha E \dot{\mathbf{v}}^0 - \tilde{c}^2(S + \beta_n \widetilde{M})\mathbf{v}^0 - \mu E \mathbf{v}^0\}, \quad (4.27)$$

where the convolution term vanishes at $t = 0$.

- (ii) For $m \geq 0$, compute \mathbf{v}^{m+1} from

$$\begin{aligned} (A + \vartheta \Delta t B + \theta \Delta t^2 C) \ddot{\mathbf{v}}^{m+1} &= \mathbf{f}^{m+1} - B(\dot{\mathbf{v}}^m + (1 - \vartheta) \Delta t \ddot{\mathbf{v}}^m) \\ &\quad - C\left(\mathbf{v}^m + \Delta t \dot{\mathbf{v}}^m + \frac{1 - 2\theta}{2} \Delta t^2 \ddot{\mathbf{v}}^m\right), \end{aligned} \quad (4.28)$$

and update \mathbf{u}^{m+1} and $\dot{\mathbf{u}}^{m+1}$ by

$$\mathbf{v}^{m+1} = \mathbf{v}^m + \Delta t \dot{\mathbf{v}}^m + \frac{1 - 2\theta}{2} \Delta t^2 \ddot{\mathbf{v}}^m + \theta \Delta t^2 \ddot{\mathbf{v}}^{m+1}, \quad (4.29)$$

$$\dot{\mathbf{v}}^{m+1} = \dot{\mathbf{v}}^m + (1 - \vartheta) \Delta t \ddot{\mathbf{v}}^m + \vartheta \Delta t \ddot{\mathbf{v}}^{m+1}, \quad (4.30)$$

respectively.

Remark 4.2. In general, the Newmark's scheme is of second-order and unconditionally stable, if the parameters satisfy $\vartheta \geq \frac{1}{2}$ and $\theta \geq \frac{1}{4}(\frac{1}{2} + \vartheta)^2$ (see, e.g., [41]).

The computational cost of the full algorithm lies in solving (4.28) with (4.26). The matrices M, \widetilde{M} and S are sparse with small bandwidth under the basis $\{\phi_k\}$, and their entries can be evaluated exactly by using the properties of Legendre polynomials. The matrices B and C in (4.26) appear to be full, but since all entries of E are one, the matrix-vector multiplication can be carried out in $O(N)$ operations. \square

5. NUMERICAL RESULTS

In this section, we present various numerical results to show the accuracy of the NRBC and convergence of the proposed algorithm.

5.1. Testing problem and setup. We examine the NRBC and the scheme via the following problem with an exact solution.

Proposition 5.1. The exterior problem (2.1)-(2.3) with $d = 2, D = \{\mathbf{x} \in \mathbb{R}^2 : |\mathbf{x}| < b_0\}, F = U_0 = U_1 \equiv 0$, and $U|_{r=b_0} = G$, admits the solution:

$$U(r, \phi, t) = \sum_{|n|=0}^{\infty} \widehat{U}_n(r, t) e^{in\phi}, \quad r > b_0, \quad \phi \in [0, 2\pi), \quad t > 0, \quad (5.1)$$

where

$$\widehat{U}_n(r, t) = \begin{cases} 0, & t < \beta_0, \\ H_n(r, t) * \widehat{G}_n(t - \beta_0) + \sqrt{b_0/r} \widehat{G}_n(t - \beta_0), & t \geq \beta_0, \end{cases} \quad (5.2)$$

with $\beta_0 = (r - b_0)/c$, $\widehat{G}_n(t)$ being the Fourier expansion coefficient of $G(\phi, t)$, and

$$\begin{aligned} H_n(r, t) &= \frac{c}{b_0} \sum_{j=1}^{M_n} \frac{K_{n+1}(r z_j^n / b_0)}{K'_n(z_j^n)} e^{tcz_j^n / b_0} \\ &\quad + (-1)^n \frac{c}{b_0} \int_0^\infty \frac{I_n(r\rho/b_0) K_n(\rho) - K_n(r\rho/b_0) I_n(\rho)}{K_n^2(\rho) + \pi^2 I_n^2(\rho)} e^{-c\rho/b_0} d\rho. \end{aligned} \quad (5.3)$$

Proof. We sketch its derivation in Appendix C. \square

Remark 5.1. Notice that \widehat{U}_n satisfies the one-dimension problem:

$$\frac{\partial^2 \widehat{U}_n}{\partial t^2} - \frac{c^2}{r} \frac{\partial}{\partial r} \left(r \frac{\partial \widehat{U}_n}{\partial r} \right) + c^2 n^2 \frac{\widehat{U}_n}{r^2} = 0, \quad b_0 < r < b, \quad t > 0; \quad (5.4)$$

$$\widehat{U}_n|_{t=0} = \frac{\partial \widehat{U}_n}{\partial t} \Big|_{t=0} = 0, \quad b_0 < r < b; \quad \widehat{U}_n|_{r=b_0} = \widehat{G}_n, \quad t > 0; \quad (5.5)$$

$$\left(\frac{1}{c} \frac{\partial \widehat{U}_n}{\partial t} + \frac{\partial \widehat{U}_n}{\partial r} + \frac{1}{2r} \widehat{U}_n \right) \Big|_{r=b} = \int_0^t \sigma_n(t-\tau) \widehat{U}_n(b, \tau) d\tau, \quad t > 0. \quad \square \quad (5.6)$$

We take the Dirichlet data:

$$G(\phi, t) = A_1 e^{-\iota((b_0 \cos \phi - x_s)^2 + (b_0 \sin \phi - y_s)^2)} \sin^p(\omega t), \quad (5.7)$$

where $A_1 = 10$, $\iota = 0.1$, $x_s = y_s = 2.1$, $b_0 = 2$, and ω, p are to be specified later. We compute the Fourier coefficient

$$\widehat{G}_n(t) = \frac{A_1}{2\pi} \sin^p(\omega t) \int_0^{2\pi} e^{-\iota((b_0 \cos \phi - x_s)^2 + (b_0 \sin \phi - y_s)^2)} e^{-in\phi} d\phi,$$

via the fast Fourier transform with sufficient Fourier points so that the error of numerical integration can be neglected.

The first important issue is to compute the exact solution and σ_n very accurately. We point out that the convolution in (5.2) can be computed exactly, and the improper integral in (5.3) can be treated by a similar manner as the improper integral of $\sigma_n(t)$ in Subsection 2.3. We adopt a Newton's iteration method to compute the zeros of $K_n(z)$ accurately for moderate large n , and use a (composite) Legendre-Gauss quadrature to evaluate the integral with high precision.

For the readers' reference, we tabulate in Table 5.1 some samples of $\sigma_n(t)$ with $b = 3$, $c = 5$.

TABLE 5.1. Some samples of $\sigma_n(t)$.

n	$\sigma_n(0.1)$	$\sigma_n(2)$	n	$\sigma_n(0.1)$	$\sigma_n(2)$
0	5.922023678764810e-2	1.127355852971518e-2	5	-5.394296605508512	2.652114252130534e-3
1	-1.770775252065292e-1	-1.849758830245009e-2	6	-7.505798337812085	-1.628640292879232e-3
2	-8.766785435408012e-1	-3.516167498630298e-3	7	-9.786660490985828	1.032611050422504e-3
3	-2.012014067208546	6.186828109004313e-3	8	-12.14241492386835	-6.793719076424341e-4
4	-3.538153424430011	-4.319820513209325e-3	9	-14.47330651171318	4.628600071971645e-4

We plot in Figure 5.1 the exact solution with $p = 2$, $b_0 = 2$, $b = 4$, $\omega = 10\pi$ at various t . We see that the Dirichlet data $G(\phi, t)$ acts as a dynamical wave-maker.

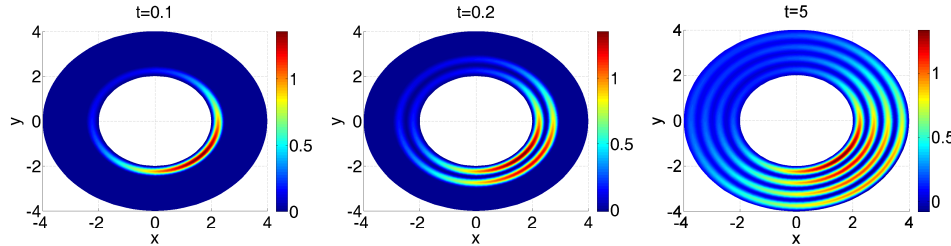


FIGURE 5.1. Time evolution of exact solution with $\omega = 10\pi$.

5.2. Accuracy of the NRBC. Now, we examine accuracy of the NRBC. Notice that

$$\max_{|\phi| \leq 2\pi} |\partial_r U_M - T_d(U_M)| \leq \sum_{|n|=0}^M e_n(t), \quad e_n(t) := \left| \left(\frac{1}{c} \frac{\partial \hat{U}_n}{\partial t} + \frac{\partial \hat{U}_n}{\partial r} + \frac{\hat{U}_n}{2r} \right) \Big|_{r=b} - \sigma_n(t) * \hat{U}_n(b, t) \right|,$$

where $T_d(U_M)$ is defined in (2.7) with $d = 2$, and $U_M(b, \phi, t) = \sum_{|n|=0}^M \hat{U}_n(b, t) e^{in\phi}$ is the truncation of the exact solution in Proposition 5.1. We choose the same parameters as those for the exact solution in Figure 5.1, and take $M = 32$ so that $\{|\hat{U}_n(b, t)|\}$ are sufficiently small for all modes $|n| \leq M$ and all t of interest. Note that the differentiations in $e_n(t)$ can be performed exactly on the exact solution.

In Table 5.2, we tabulate the errors:

$$E_M^{(1)}(t) = \max_{|n| \leq M} e_n(t), \quad E_M^{(2)}(t) = \sum_{|n|=0}^M e_n(t),$$

at some samples of t , compute the errors at the outer artificial boundary $r = b$, where the exact solution has the magnitude as large as possible.

TABLE 5.2. The errors $E_M^{(1)}(t)$ and $E_M^{(2)}(t)$.

t	$\omega = 10\pi, b = 2.22$		$\omega = 10\pi, b = 2.75$		$\omega = 20\pi, b = 2.38$		$\omega = 20\pi, b = 2.87$	
	$E_M^{(1)}(t)$	$E_M^{(2)}(t)$	$E_M^{(1)}(t)$	$E_M^{(2)}(t)$	$E_M^{(1)}(t)$	$E_M^{(2)}(t)$	$E_M^{(1)}(t)$	$E_M^{(2)}(t)$
0.5	2.637e-16	4.902e-16	7.026e-17	1.148e-16	6.245e-17	1.603e-16	8.327e-17	1.752e-16
1	4.684e-16	8.406e-16	2.099e-16	2.630e-16	9.021e-17	2.390e-16	2.272e-16	4.405e-16
5	2.567e-16	4.386e-16	1.131e-15	1.176e-15	7.251e-16	9.053e-16	1.318e-15	1.473e-15
10	7.772e-16	1.020e-15	2.207e-15	2.227e-15	1.457e-15	1.960e-15	2.387e-15	2.575e-15

We see from Table 5.2 that in all tests, the errors are extremely small. This validates the formula for σ_n in Theorem 2.1 and high accuracy of the numerical treatment.

5.3. Numerical tests for the spectral-Galerkin-Newmark's scheme. Hereafter, we provide some numerical results to illustrate the convergence of the numerical scheme described in Section 4. In the following computations, we take the Dirichlet data given by (5.7) with $A_1 = 10, \iota = 0.1, x_s = y_s = 2.1$ and $b_0 = 2$ as before.

Given a cut-off number $M > 0$, we compute the numerical solutions $\{\hat{U}_n^N\}$ of (5.4)-(5.6) for the modes $|n| \leq M$ by using the spectral-Galerkin and Newmark's time integration scheme. The full numerical solution of the problem in Proposition 5.1 is then defined as $U_M^N(r, \phi, t) = \sum_{|n|=0}^M \hat{U}_n^N(r, t) e^{in\phi}$, and the exact solution $U_M(r, \phi, t) = \sum_{|n|=0}^M \hat{U}_n(r, t) e^{in\phi}$ is evaluated as before. Once again, we choose M such that the Fourier coefficient of the exact solution $|\hat{U}_n| \leq 10^{-16}$ for $|n| > M$. The numerical errors are measured by

$$\hat{E}_M^N(t) = \max_{|n| \leq M} \|\hat{U}_n^N(\cdot, t) - \hat{U}_n(\cdot, t)\|_{L^2, N}, \quad \tilde{E}_M^N(t) = \max_{|n| \leq M} \|\hat{U}_n^N(\cdot, t) - \hat{U}_n(\cdot, t)\|_{L^\infty, N},$$

where $\|\cdot\|_{L^2, N}$ is the discrete L^2 -norm associated with the Legendre-Gauss-Lobatto interpolation, and $\|\cdot\|_{L^\infty, N}$ is the corresponding discrete maximum norm.

To test the second-order convergence of the Newmark's scheme, we choose $N = 50$ so that the error of the spatial discretization is negligible. We provide in Table 5.3 the numerical errors and the order of convergence for various t with $M = 15, b = 5, \omega = \pi$, and $p = 6$. As expected, we observe a second-order convergence of the time integration.

Next, we fix the time step size $\Delta t = 10^{-5}$ and choose different N to check the accuracy in spatial discretization. The convergence behavior is illustrated in Table 5.3. With a small

TABLE 5.3. The errors $\hat{E}_M^N(t)$ and $\tilde{E}_M^N(t)$, and order of convergence.

t	Δt	$\hat{E}_M^N(t)$	order	$\tilde{E}_M^N(t)$	order	t	Δt	$\hat{E}_M^N(t)$	order	$\tilde{E}_M^N(t)$	order
1	1e-03	1.21e-05		1.93e-05		3	1e-03	1.23e-05		2.01e-05	
	5e-04	3.02e-06	2.00005	4.83e-06	1.99994		5e-04	3.07e-06	2.00007	5.02e-06	1.99997
	1e-04	1.21e-07	1.99993	1.93e-07	1.99986		1e-04	1.23e-07	1.99997	2.01e-07	1.99998
	5e-05	3.02e-08	2.00012	4.83e-08	1.99906		5e-05	3.07e-08	2.00007	5.02e-08	2.00004
	1e-03	1.23e-05		2.01e-05			1e-03	1.23e-05		2.01e-05	
2	5e-04	3.07e-06	1.99998	5.02e-06	1.99997	4	5e-04	3.07e-06	2.00007	5.02e-06	1.99997
	1e-04	1.23e-07	2.00001	2.01e-07	1.99998		1e-04	1.23e-07	1.99997	2.01e-07	1.99998
	5e-05	3.07e-08	2.00002	5.02e-08	1.99993		5e-05	3.07e-08	2.00007	5.02e-08	2.00004

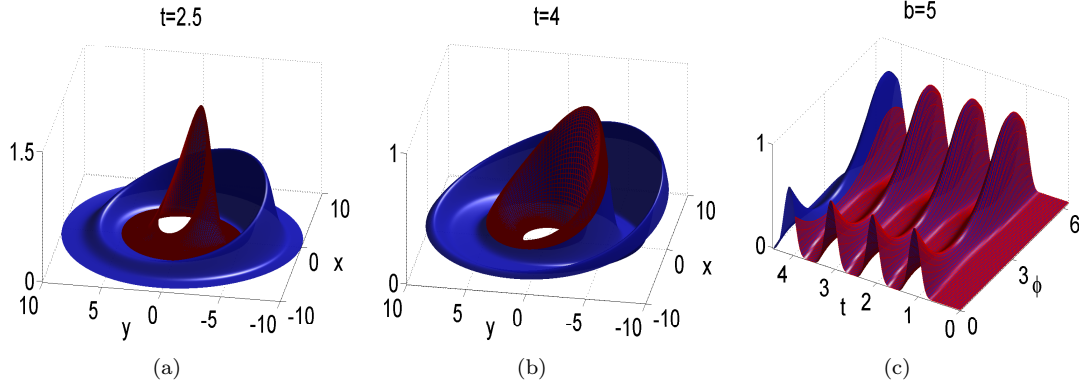


FIGURE 5.2. Propagation of exact and numerical solutions.

number of modes in space, we observe a fast decay of the errors, which is typical for the spectral approximation.

TABLE 5.4. The errors $\hat{E}_M^N(t)$ and $\tilde{E}_M^N(t)$.

t	$N = 8$		$N = 10$		$N = 16$		$N = 32$	
	$\hat{E}_M^N(t)$	$\tilde{E}_M^N(t)$	$\hat{E}_M^N(t)$	$\tilde{E}_M^N(t)$	$\hat{E}_M^N(t)$	$\tilde{E}_M^N(t)$	$\hat{E}_M^N(t)$	$\tilde{E}_M^N(t)$
0.5	2.349e-04	2.687e-04	2.253e-05	2.846e-05	8.224e-07	1.207e-06	9.229e-09	1.639e-08
1.0	3.877e-04	4.179e-04	1.708e-05	2.042e-05	1.833e-07	2.777e-07	1.959e-09	2.673e-09
1.5	3.276e-04	3.596e-04	5.965e-06	7.146e-06	3.072e-08	5.238e-08	1.508e-09	1.762e-09
2.0	4.105e-04	4.368e-04	1.092e-05	1.188e-05	7.353e-09	1.238e-08	1.237e-09	2.119e-09
2.5	3.239e-04	3.607e-04	5.724e-06	6.997e-06	2.381e-09	3.182e-09	1.488e-09	1.734e-09
3.0	4.113e-04	4.380e-04	1.095e-05	1.189e-05	1.404e-09	2.893e-09	1.227e-09	2.009e-09
3.5	3.238e-04	3.608e-04	5.747e-06	7.036e-06	1.554e-09	2.063e-09	1.488e-09	1.732e-09
4.0	4.113e-04	4.380e-04	1.095e-05	1.189e-05	1.269e-09	2.061e-09	1.227e-09	2.007e-09

Finally, we plot in Figure 5.2 the numerical solution (red nets) against the exact solution (blue smooth surface), where the exact solution in (a) and (b) is in the annulus: $2 \leq r \leq 10$, while the numerical solution within $2 \leq r \leq 5$. Figure 5.2(c) shows the wave propagation through the artificial boundary at $b = 5$, $0 \leq \phi \leq 2\pi$ for $0 \leq t \leq 4$ (numerical solution) against $0 \leq t \leq 4.5$ (exact solution). We see that the red nets and blue surfaces agree well in these plots. Moreover, we observe the waves pass the boundary transparently. This shows that the proposed scheme is very stable and has high-order accuracy.

Concluding remarks

We proposed in this paper analytic and accurate numerical means for the time-domain wave propagation with exact and global nonreflecting boundary conditions. We derived the analytic expressions of the convolution kernels and presented highly accurate methods for their evaluations. We analyzed the stability of the truncated problem and provided efficient numerical schemes. Ample numerical results were given to demonstrate the features of the method. We shall report the combination of the methods with the boundary perturbation technique in a future work. The techniques and ideas in this paper will be useful to study the Maxwell equations and elastic wave propagations.

APPENDIX A. PROOF OF THEOREM 2.1

We first consider $d = 2$. Note that $F_n(z)$ is a multi-valued function with branch points at $z = 0$ and infinity. The contour L for (2.15) is depicted in Figure A.1 (left) with the branch-cut along the negative real axis.

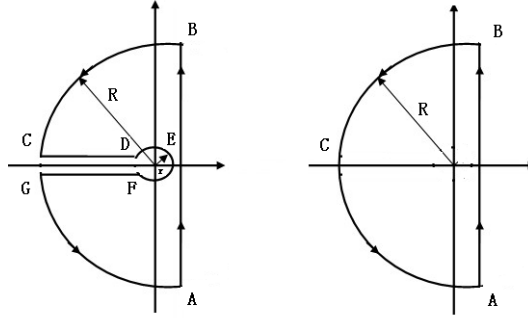


FIGURE A.1. Contour L for the inverse Laplace transform. Left: $d = 2$. Right: $d = 3$.

We know from Lemma 2.1 that $F_n(z)$ has a finite number of simple poles in the second and third quadrants, Therefore, for any $n \geq 0$, it follows from the residue theorem that

$$\begin{aligned} \lim_{\substack{R \rightarrow +\infty \\ r \rightarrow 0^+}} \oint_L F_n(z) e^{czt/b} dz &= 2\pi i \sum_{j=1}^{M_n} \text{Res} [F_n(z) e^{czt/b}, z_j^n] \\ &= 2\pi i \sum_{j=1}^{M_n} \lim_{z \rightarrow z_j^n} \left\{ (z - z_j^n) e^{czt/b} \left[z + \frac{1}{2} + z \frac{K'_n(z)}{K_n(z)} \right] \right\} = 2\pi i \sum_{j=1}^{M_n} e^{ctz_j^n/b} z_j^n. \end{aligned} \quad (\text{A.1})$$

Thus, by (2.15) and (A.1),

$$\begin{aligned} \frac{2b^2\pi i}{c} \sigma_n(t) &= 2\pi i \sum_{j=1}^{M_n} e^{ctz_j^n/b} z_j^n - \lim_{\substack{R \rightarrow +\infty \\ r \rightarrow 0^+}} \left[\int_{\widehat{BC}} F_n(z) e^{czt/b} dz + \int_{\widehat{CD}} F_n(z) e^{czt/b} dz \right. \\ &\quad \left. + \int_{\widehat{DEF}} F_n(z) e^{czt/b} dz + \int_{\widehat{FG}} F_n(z) e^{czt/b} dz + \int_{\widehat{GA}} F_n(z) e^{czt/b} dz \right]. \end{aligned} \quad (\text{A.2})$$

In view of (2.14), we find from the Jordan's lemma (cf. [11, 8]) and a direct calculation that

$$\lim_{\substack{R \rightarrow +\infty \\ r \rightarrow 0^+}} \left[\int_{\widehat{BC}} F_n(z) e^{czt/b} dz + \int_{\widehat{DEF}} F_n(z) e^{czt/b} dz + \int_{\widehat{GA}} F_n(z) e^{czt/b} dz \right] = 0, \quad (\text{A.3})$$

since each contour integral tends to zero. Thus, we only need to evaluate the integrals along the line segments \overline{CD} and \overline{FG} . We have

$$\lim_{\substack{R \rightarrow +\infty \\ r \rightarrow 0^+}} \left[\int_{\overline{CD}} F_n(z) e^{czt/b} dz + \int_{\overline{FG}} F_n(z) e^{czt/b} dz \right] = \int_0^\infty r e^{-ctr/b} \left[\frac{K'_n(re^{-i\pi})}{K_n(re^{-i\pi})} - \frac{K'_n(re^{i\pi})}{K_n(re^{i\pi})} \right] dr.$$

By Formula 9.6.31 of [1],

$$K_n(re^{\pi i}) = e^{-n\pi i} K_n(r) - \pi i I_n(r), \quad K_n(re^{-\pi i}) = e^{n\pi i} K_n(r) + \pi i I_n(r),$$

which, together with (2.13), implies

$$\begin{aligned} \frac{K'_n(re^{i\pi})}{K_n(re^{i\pi})} - \frac{K'_n(re^{-i\pi})}{K_n(re^{-i\pi})} &= \frac{K_{n+1}(re^{-i\pi})}{K_n(re^{-i\pi})} - \frac{K_{n+1}(re^{i\pi})}{K_n(re^{i\pi})} \\ &= \frac{e^{(n+1)\pi i} K_{n+1}(r) + \pi i I_{n+1}(r)}{e^{n\pi i} K_n(r) + \pi i I_n(r)} - \frac{e^{-(n+1)\pi i} K_{n+1}(r) - \pi i I_{n+1}(r)}{e^{-n\pi i} K_n(r) - \pi i I_n(r)} \\ &= \frac{(-1)^n 2\pi i [K_{n+1}(r) I_n(r) + K_n(r) I_{n+1}(r)]}{K_n^2(r) + \pi^2 I_n^2(r)} = \frac{(-1)^n 2\pi i}{r [K_n^2(r) + \pi^2 I_n^2(r)]}, \end{aligned} \quad (\text{A.4})$$

where we used the Wronskian identity (see Formula 9.6.15 of [1]):

$$I_n(z) K_{n+1}(z) + I_{n+1}(z) K_n(z) = z^{-1}. \quad (\text{A.5})$$

A combination of (A.1)-(A.4) leads to

$$\sigma_n(t) = \frac{c}{b^2} \left\{ \sum_{j=1}^{M_n} z_j^n e^{ctz_j^n/b} + \int_0^\infty \frac{(-1)^n e^{-ctr/b}}{K_n^2(r) + \pi^2 I_n^2(r)} dr \right\}, \quad (\text{A.6})$$

which is the expression (2.19).

Now, we turn to the three dimensional case. It is important to notice that the kernel function $F_{n+1/2}(z)$ is not a multi-valued complex function, as opposed to the two dimensional case. Indeed, although $K_{n+1/2}(z)$ is multi-valued, in view of the formula (see Page 80 of [40]):

$$K_{n+1/2}(z) = \sqrt{\frac{\pi}{2z}} \sum_{k=0}^n \frac{(n+k)! e^{-z}}{k!(n-k)!(2z)^k}, \quad \forall n \geq 0, \quad (\text{A.7})$$

the fact $1/\sqrt{z}$ can be eliminated from the ratio $K'_{n+1/2}/K_{n+1/2}$. Thanks to this property, we use the contour in Figure A.1 (right), by the residue theorem and Jordan's lemma, we have

$$\begin{aligned} \lim_{R \rightarrow +\infty} \oint_L F_{n+1/2}(z) e^{czt/b} dz &= \int_{\gamma - \infty i}^{\gamma + \infty i} F_{n+1/2}(z) e^{czt/b} dz \\ &= 2\pi i \sum_{j=1}^{M_\nu} \text{Res} [F_{n+1/2}(z) e^{czt/b}, z_j^\nu] = 2\pi i \sum_{j=1}^{M_\nu} e^{ctz_j^\nu/b} z_j^\nu, \end{aligned} \quad (\text{A.8})$$

for $\nu = n + 1/2$. This leads to the formula (2.20). \square

APPENDIX B. JUSTIFICATION FOR REMARK 2.3

Thanks to (2.17), we have

$$z \frac{H_\nu^{(1)'}(z)}{H_\nu^{(1)}(z)} = -iz \frac{K'_\nu(-iz)}{K_\nu(-iz)}.$$

Thus, by (2.21) with $\nu = n$ and $-iz = bs/c$, we find

$$\frac{s}{c} + \frac{1}{2b} + \frac{s}{c} \frac{K'_n(bs/c)}{K_n(bs/c)} = -\frac{ic}{b^2} \sum_{j=1}^{N_n} \frac{h_{n,j}}{s + \frac{ich_{n,j}}{b}} + \frac{c}{b^2} \int_0^\infty \frac{(-1)^n}{K_n^2(r) + \pi^2 I_n^2(r)} \frac{1}{\frac{cr}{b} + s} dr.$$

Applying the inverse Laplace transform to both sides of the above identity leads to

$$\mathcal{L}^{-1} \left[\frac{s}{c} + \frac{1}{2b} + \frac{s}{c} \frac{K'_n(bs/c)}{K_n(bs/c)} \right] = \frac{c}{b^2} \sum_{j=1}^{N_n} (-ih_{n,j}) e^{-ict h_{n,j}/b} + \frac{c}{b^2} \int_0^\infty \frac{(-1)^n e^{-crt/b}}{K_n^2(r) + \pi^2 I_n^2(r)} dr,$$

which turns out to be (A.6), since $-ih_{n,j}$ are zeros of $K_n(z)$ and $N_n = M_n$. \square

APPENDIX C. PROOF OF PROPOSITION 5.1

This problem can be solved by Laplace transform and separation of variables. Indeed, the Fourier coefficients $\{\widehat{U}_n\}$ in (5.1) can be expressed as

$$\widehat{U}_n(r, t) = \mathcal{L}^{-1} \left(\frac{K_n(sr/c)}{K_n(sb_0/c)} \right) (t) * \widehat{G}_n(t), \quad r > b_0. \quad (\text{C.1})$$

We next sketch the evaluation of the inverse Laplace transform by using the residue theorem as in Appendix A for $\sigma_n(t)$. Using (2.12), we find $\frac{K_n(sr/c)}{K_n(sb_0/c)} \sim \sqrt{\frac{b_0}{r}} e^{-s\beta_0}$, where $\beta_0 = (r - b_0)/c$. In order to use the Jordan's lemma (cf. [11, 8]), we write

$$\begin{aligned} \mathcal{L}^{-1} \left(\frac{K_n(sr/c)}{K_n(sb_0/c)} \right) (t) &= \mathcal{L}^{-1} \left(e^{-\beta_0 s} \left\{ e^{\beta_0 s} \frac{K_n(sr/c)}{K_n(sb_0/c)} - \sqrt{\frac{b_0}{r}} \right\} \right) + \mathcal{L}^{-1} \left(e^{-\beta_0 s} \sqrt{\frac{b_0}{r}} \right) (t) \\ &= \widetilde{H}_n(r, t - \beta_0) U_{\beta_0}(t) + \sqrt{\frac{b_0}{r}} \delta(t - \beta_0), \end{aligned} \quad (\text{C.2})$$

where $\widetilde{H}_n(r, t) = \mathcal{L}^{-1} \left(e^{\beta_0 s} \frac{K_n(sr/c)}{K_n(sb_0/c)} - \sqrt{b_0/r} \right) (t)$, $U_{\beta_0}(t)$ is the unit step function (which takes 1 for $t \geq \beta_0$, and 0 for $t < \beta_0$), and $\delta(t)$ is the Dirac delta function. By applying the residue theorem and Jordan's lemma to the Bromwich's contour integral:

$$\widetilde{H}_n(r, t) = \frac{1}{2\pi i} \int_{\gamma - \infty i}^{\gamma + \infty i} \left(e^{\beta_0 s} \frac{K_n(sr/c)}{K_n(sb_0/c)} - \sqrt{\frac{b_0}{r}} \right) e^{ts} ds, \quad (\text{C.3})$$

we obtain (5.3) by using the contour in Figure A.1 (left) and the same argument as in Appendix A. Denoting $H_n(r, t) := \widetilde{H}_n(r, t - \beta_0)$, the expression (5.2) follows from (C.2). We leave the details to the interested readers. \square

REFERENCES

- [1] M. Abramowitz and I.A. Stegun, editors. *Handbook of Mathematical Functions with Formulas, Graphs, and Mathematical Tables*. A Wiley-Interscience Publication. John Wiley & Sons Inc., New York, 1984. Reprint of the 1972 edition, Selected Government Publications.
- [2] B. Alpert, L. Greengard, and T. Hagstrom. Rapid evaluation of nonreflecting boundary kernels for time-domain wave propagation. *SIAM J. Numer. Anal.*, 37(4):1138–1164 (electronic), 2000.
- [3] B. Alpert, L. Greengard, and T. Hagstrom. Nonreflecting boundary conditions for the time-dependent wave equation. *J. Comput. Phys.*, 180(1):270–296, 2002.
- [4] A. Bayliss and E. Turkel. Radiation boundary conditions for wave-like equations. *Comm. Pure Appl. Math.*, 33(6):707–725, 1980.
- [5] J.P. Berenger. A perfectly matched layer for the absorption of electromagnetic waves. *J. Comput. Phys.*, 114(2):185–200, 1994.
- [6] Z.M. Chen. Convergence of the time-domain perfectly matched layer method for acoustic scattering problems. *Int. J. Numer. Anal. Model.*, 6(1):124–146, 2009.
- [7] R.D. Ciskowski and C.A. Brebbia. *Boundary Element Methods in Acoustics*. Kluwer Academic Publishers, 1991.
- [8] A.M. Cohen. *Numerical Methods for Laplace Transform Inversion*, volume 5 of *Numerical Methods and Algorithms*. Springer, New York, 2007.
- [9] G.C. Cohen. *Higher-Order Numerical Methods for Transient Wave Equations*. Scientific Computation. Springer-Verlag, Berlin, 2002. With a foreword by R. Glowinski.
- [10] M.D. Collins and W.A. Kuperman. Inverse problems in ocean acoustics. *Inverse Problems*, 10(5):1023–1040, 1994.

- [11] B. Davies. *Integral Transforms and Their Applications*, volume 41 of *Texts in Applied Mathematics*. Springer-Verlag, New York, third edition, 2002.
- [12] B. Engquist and A. Majda. Absorbing boundary conditions for the numerical simulation of waves. *Math. Comp.*, 31(139):629–651, 1977.
- [13] Q.R. Fang, D.P. Nicholls, and J. Shen. A stable, high-order method for three-dimensional, bounded-obstacle, acoustic scattering. *J. Comput. Phys.*, 224(2):1145–1169, 2007.
- [14] K. Gerdes and L. Demkowicz. Solution of 3D-Laplace and Helmholtz equations in exterior domains using *hp*-infinite elements. *Comput. Methods Appl. Mech. Engrg.*, 137(3-4):239–273, 1996.
- [15] D. Givoli. *Numerical Methods for Problems in Infinite Domains*, volume 33 of *Studies in Applied Mechanics*. Elsevier Scientific Publishing Co., Amsterdam, 1992.
- [16] D. Givoli. High-order local non-reflecting boundary conditions: a review. *Wave Motion*, 39(4):319–326, 2004. New computational methods for wave propagation.
- [17] M.J. Grote and J.B. Keller. Exact nonreflecting boundary conditions for the time-dependent wave equation. *SIAM J. Appl. Math.*, 55(2):280–297, 1995.
- [18] T. Hagstrom. Radiation boundary conditions for the numerical simulation of waves. In *Acta numerica, 1999*, volume 8 of *Acta Numer.*, pages 47–106. Cambridge Univ. Press, Cambridge, 1999.
- [19] R.N. Huan and L.L. Thompson. Accurate radiation boundary conditions for the time-dependent wave equation on unbounded domains. *Internat. J. Numer. Methods Engrg.*, 47(9):1569–1603, 2000.
- [20] S.D. Jiang and L. Greengard. Fast evaluation of nonreflecting boundary conditions for the Schrödinger equation in one dimension. *Comput. Math. Appl.*, 47(6-7):955–966, 2004.
- [21] S.D. Jiang and L. Greengard. Efficient representation of nonreflecting boundary conditions for the time-dependent Schrödinger equation in two dimensions. *Comm. Pure Appl. Math.*, 61(2):261–288, 2008.
- [22] J.B. Keller and D. Givoli. Exact nonreflecting boundary conditions. *J. Comput. Phys.*, 82(1):172–192, 1989.
- [23] J.R. Li. Low order approximation of the spherical nonreflecting boundary kernel for the wave equation. *Linear Algebra Appl.*, 415(2-3):455–468, 2006.
- [24] C. Lubich and A. Schädle. Fast convolution for nonreflecting boundary conditions. *SIAM J. Sci. Comput.*, 24(1):161–182 (electronic), 2002.
- [25] P.A. Martin. *Multiple Scattering: Interaction of Time-Harmonic Waves with N Obstacles*, volume 107. Cambridge University Press, 2006.
- [26] J.C. Nédélec. *Acoustic and Electromagnetic Equations*, volume 144 of *Applied Mathematical Sciences*. Springer-Verlag, New York, 2001. Integral representations for harmonic problems.
- [27] N.M. Newmark. A method of computation for structural dynamics. In *Proc. ASCE*, volume 85, pages 67–94, 1959.
- [28] D. Nicholls and F. Reitich. Analytic continuation of Dirichlet-Neumann operators. *Numer. Math.*, 94(1):107–146, 2003.
- [29] D. Nicholls and J. Shen. A stable, high-order method for two-dimensional bounded-obstacle scattering. *SIAM J. Sci. Comput.*, 28:1398–1419, 2006.
- [30] D. Nicholls and J. Shen. A rigorous numerical analysis of the transformed field expansion method. *SIAM J. Numer. Anal.*, 47(4):2708–2734, 2009.
- [31] J. Shen. Efficient spectral-Galerkin method I. direct solvers for second- and fourth-order equations by using Legendre polynomials. *SIAM J. Sci. Comput.*, 15:1489–1505, 1994.
- [32] J. Shen, T. Tang, and L.L. Wang. *Spectral Methods: Algorithms, Analysis and Applications*, volume 41 of *Springer Series in Computational Mathematics*. Springer-Verlag, Berlin, Heidelberg, 2011.
- [33] K.L. Shlager and J.B. Schneider. A selective survey of the finite-difference time-domain literature. *Antennas and Propagation Magazine, IEEE*, 37(4):39–57, 1995.
- [34] I.L. Sofronov. Conditions for complete transparency on a sphere for a three-dimensional wave equation. *Dokl. Akad. Nauk*, 326(6):953–957, 1992.
- [35] I.L. Sofronov. Artificial boundary conditions of absolute transparency for two- and three-dimensional external time-dependent scattering problems. *European J. Appl. Math.*, 9(6):561–588, 1998.
- [36] G. Szegő. *Orthogonal Polynomials (Fourth Edition)*, volume 23. AMS Coll. Publ., 1975.
- [37] A. Taflov and S.C. Hagness. *Computational Electrodynamics: the Finite-Difference Time-Domain Method*. Artech House Inc., Boston, MA, third edition, 2005. With 1 CD-ROM (Windows).
- [38] L.L. Thompson and R.N. Huan. Computation of far-field solutions based on exact nonreflecting boundary conditions for the time-dependent wave equation. *Comput. Methods Appl. Mech. Engrg.*, 190(11-12):1551–1577, 2000.
- [39] L. Ting and M.J. Miksis. Exact boundary conditions for scattering problems. *The Journal of the Acoustical Society of America*, 80:1825, 1986.
- [40] G.N. Watson. *A Treatise of the Theory of Bessel Functions (second edition)*. Cambridge University Press, Cambridge, UK, 1966.
- [41] W.L. Wood. *Practical Time-Stepping Schemes*. Oxford Applied Mathematics and Computing Science Series. The Clarendon Press Oxford University Press, New York, 1990.